Balancing Legged Robots on Visco-Elastic Contacts

Thomas Flayols, Andrea del Prete, Majid Khadiv, Nicolas Mansard, Ludovic
Righetti

Balancing Legged Robots on Visco-Elastic Contacts

Thomas Flayols[1], Andrea Del Prete[2], Majid Khadiv[3], Nicolas Mansard[1], and Ludovic Righetti[3,4]

Abstract—Contacts between robots and environment are often assumed to be rigid for control purposes. This assumption can lead to poor performance when contacts are soft and/or under-damped. However, the problem of balancing on soft contacts has not received much attention in the literature. This paper discusses four approaches to control a legged robot balancing on visco-elastic contacts. Two of these approaches are novel, whereas the other two are taken from the state of the art. Our simulation results show that no approach can outperform all the others in all situations. Performance heavily depends on the contact stiffness and the noises/uncertainties introduced in the simulation. These results sheds light on this challenging problem, while pointing out interesting directions for future investigation.

Index Terms—IEEE, IEEEtran, journal, LATEX, paper, template.

I. INTRODUCTION

A. Problem Overview

The problem of balancing is fundamental for any legged robotic system and it has received much attention in the literature [1]. However, most people have focused on balancing a *rigid* robot in contact with a *rigid* environment [2], [3], [4], [5], [6], [7]. In this scenario, in theory, we can instantaneously change the contact forces exerted between robot and environment. This is no longer the case if the environment is visco-elastic, or, equivalently, a *visco-elastic element* is located between the robot actuators and the contact points. This is the case of many legged robots, which are equipped with visco-elastic elements in the proximity of their feet [8], [9], [7], [10]. These elements are extremely useful: they absorb impacts during walking/running, protect the mechanical structure, tend to improve the quality of force measurements, and can make walking more efficient [10]. Moreover, the assumption of rigid contact is always an approximation because in the real world all contacts are visco-elastic—to a certain extent. In the presence of *elasticity*, we can no longer instantaneously change the contact forces, but only their derivative—either first or second, depending on the contact damping (as we detail in Section II). Despite the popularity of visco-elastic elements, balancing on visco-elastic contacts is still an open problem.

B. State of the Art

The classic approach is to neglect elasticity in the balance controller, and simply assume that contacts are rigid. This

[1]CNRS, LAAS, 7 avenue du colonel Roche, Univ de Toulouse, LAAS, F-31400 Toulouse, France, tflayols@laas.fr, nmansard@laas.fr
[2]Industrial Engineering Department, University of Trento, Italy, andrea.delprete@unitn.it
[3]Max Planck Institute for Intelligent Systems, Tuebingen, Germany, mkhadiv@tue.mpg.de, lrighetti@tue.mpg.de
[4]Tandon School of Engineering, New York University, USA

works fine for contacts that are not too soft and that are sufficiently damped, as it has been demonstrated with a passivity-based controller on the Toro humanoid robot [11]. However, in general, this can result in destabilizing oscillations [1]. Force feedback can then be used to damp these oscillations. The most common approach is to use force feedback to modify the position references given to a high-gain joint position controller, leading to admittance control schemes [9], [7], [5]. While this approach proved successful in practice, it lacks theoretical foundations, which makes it challenging to tune and analyze.

A crucial issue of admittance control schemes is the resulting delay in the force tracking. In order to deal with it, two approaches have been proposed. The first one [3] is to prove that the controller is robust to these delays. The second method [8] is to model the delay as a 1-st order low-pass filter, and account for it in the dynamic model used in the balance controller. Our analysis reveals that actually the force tracking delay is not an issue, as long as the admittance control gains are properly set.

Instead of relying on admittance control schemes, another approach [12] tries to change the contact forces at the next time step—since we cannot change them instantaneously. This approach exploits a model of the visco-elastic contacts for the controller design. However, it mainly relies on contact damping, thus it cannot be applied if damping is too low (see Section II-A).

Recently, the state-of-the-art Whole-Body Controller [13] has been extended to ensure consistency to terrain compliance [14]. This controller incorporates a soft contact model and is connected with an online learning algorithm that estimates the terrain compliance. This work has focused on well damped contacts, whereas we focus here on the under-damped case.

C. Contributions

Our main contributions are two novel approaches to control a legged robot on visco-elastic contacts. Our approaches rely on an explicit model of the visco-elastic contacts. This allows us to unify position and force feedback, leading to a simple gain tuning procedure, for which we can rely on standard linear system techniques (e.g., LQR, pole placement). Our second contribution is a thorough comparison of the two novel controllers with two state-of-the-art approaches through noisy simulations. This highlights pros and cons of each method according to the contact stiffness.

D. Paper Structure

Section II introduces the visco-elastic contact model and the robot dynamics. Section III presents a novel approach

to balance on elastic contacts (TSID-Flex-K). Then, the next two sections summarize two state-of-the-art methods. The first one (Section IV) is classically used for rigid contacts (TSID-Rigid [4]). The second one (Section V) is an admittance control scheme (Adm-Ctrl) relying on joint position control [8]. Section VI presents an extension of Adm-Ctrl (TSID-Adm). For all methods (except for Adm-Ctrl) we present an automatic gain tuning procedure (Section VII). Section VIII discusses the estimation problem. Then Section IX discusses simulation results comparing the four methods. Finally, Section X concludes the paper.

II. ROBOT DYNAMICS AND CONTACT MODEL

A. Visco-Elastic Contact Model

Consider a robot in contact with the environment at k contact points. We assume that the contact surfaces are visco-elastic, or, equivalently, the robot is equipped with visco-elastic elements between each contact point and the last actuator of the corresponding kinematic chain. In the latter case, we can model the part of the robot after the visco-elastic element as part of the environment, and the contact point as the last point of the robot before the visco-elastic element. We also assume that each contact force $f_i \in \mathbb{R}^3$ is proportional to the associated contact position $p_i \in \mathbb{R}^3$ and velocity $\dot{p}_i \in \mathbb{R}^3$:

$$f_i = K_i(p_i^0 - p_i) - B_i \dot{p}_i, \qquad \forall i \in [1, k] \tag{1}$$

where $K_i, B_i \in \mathbb{R}^{3 \times 3}$ are the positive-definite diagonal stiffness and damping matrices, respectively, and $p_i^0 \in \mathbb{R}^3$ is the contact position corresponding to a null force. Stacking all contact forces together we can rewrite (1) as:

$$f = K(p_0 - p) - B\dot{p} \tag{2}$$

Given that contacts are unilateral, this model is valid as long as normal forces are positive (i.e., pushing). Since the contact forces are a function of the robot configuration, we cannot change them instantaneously as in the rigid contact case. However, if $B \neq 0$, we can affect their time derivative through the contact point accelerations $\ddot{p}$:

$$\dot{f} = -K\dot{p} - B\ddot{p} \tag{3}$$

If instead $B \approx 0$, we can only affect the second time derivative of f:

$$\ddot{f} = -K\ddot{p} \tag{4}$$

B. Importance of Stiffness VS Damping

Our main interest lies in the underdamped case—which is more challenging in our experience—which means that $B \ll 2\sqrt{K}$. In these cases, relying on (3) to control $\dot{f}$ may not be convenient because very large values of $\ddot{p}$ (hence motor commands) may be required. For instance, let us assume that the desired CoM trajectory $c^*(t)$ is a sinusoid with frequency $\frac{\omega_c}{2\pi}$ Hz and amplitude ψ.

$$c^*(t) = \psi \sin(\omega_c t) \tag{5}$$

Since the CoM acceleration $\ddot{c}$ is an affine function of the contact forces f, their time derivatives are also linearly related.

$$\dot{f}^*(t) \propto \dddot{c}^*(t) = -\psi \omega_c^3 \cos(\omega_c t)$$
$$\ddot{f}^*(t) \propto \ddddot{c}^*(t) = \psi \omega_c^4 \sin(\omega_c t) \tag{6}$$

Thus, relying on (3) to control $\dot{f}$ we would get:

$$\ddot{p}^*(t) \propto B^{-1} \dot{f}^*(t) \propto B^{-1} \psi \omega_c^3 \tag{7}$$

If we relied instead on (4) (i.e. neglecting the contact damping) we would get:

$$\ddot{p}^*(t) \propto K^{-1} \ddot{f}^*(t) \propto K^{-1} \psi \omega_c^4 \tag{8}$$

The latter approach results in smaller values of $\ddot{p}^*$ if this condition is satisfied:

$$K^{-1} \psi \omega_c^4 < B^{-1} \psi \omega_c^3$$
$$\zeta < \frac{\sqrt{K}}{2\omega_c}, \tag{9}$$

where the damping ratio ζ is defined as the ratio between B and the critical damping (i.e. $B \triangleq \zeta 2\sqrt{K}$). Since typically $K > 10^4$, while $\zeta < 1$ and $\omega_c < 30$, this condition is usually satisfied. For this reason, we prefer to rely on (4) rather than on (3) for our controller design.

C. Centroidal Dynamics

In order to balance a legged robot we have to control its CoM c and its angular momentum l. The dynamics of these two quantities is described by the Newton-Euler equations, where all quantities are expressed in an arbitrary inertial frame having z aligned with gravity:

$$m\ddot{c} = \sum_{i=1}^{k} f_i + mg \tag{10a}$$

$$\dot{l} = \sum_{i=1}^{k} (p_i - c) \times f_i \tag{10b}$$

where $m \in \mathbb{R}$ is the robot mass, and $g = (0, 0, -9.81)$ is the gravity acceleration. We can write (10) in matrix form as:

$$\underbrace{\begin{bmatrix} m\ddot{c} \\ \dot{l} \end{bmatrix}}_{\ddot{x}} = \underbrace{\begin{bmatrix} I_3 & \cdots & I_3 \\ [(p_1 - c)\times] & \cdots & [(p_k - c)\times] \end{bmatrix}}_{A} \underbrace{\begin{bmatrix} f_1 \\ \vdots \\ f_k \end{bmatrix}}_{f} + \underbrace{\begin{bmatrix} mg \\ 0_3 \end{bmatrix}}_{b},$$
$$\tag{11}$$

where $[y\times] \in \mathbb{R}^{3 \times 3}$ is the cross-product matrix associated to y.

D. Whole Body Dynamics

The dynamics of a floating-base robot with n joints is described by the following equations:

$$M\dot{v} + h - J^\top f = S^\top \tau, \tag{12}$$

where $M \in \mathbb{R}^{(n+6) \times (n+6)}$ is the mass matrix, $v \in \mathbb{R}^{n+6}$ is the robot velocity vector, $h \in \mathbb{R}^{n+6}$ contains the bias forces, $J \in \mathbb{R}^{3k \times (n+6)}$ is the contact Jacobian,

$S = \begin{bmatrix} 0_{n \times 6} & I_{n \times n} \end{bmatrix} \in \mathbb{R}^{n \times (n+6)}$ is a selection matrix, and $\tau \in \mathbb{R}^n$ are the joint torques. The same dynamics can be expressed by splitting the first 6 rows, which correspond to the unactuated floating base, from the last n rows, which correspond to the actuated joints:

$$M_u \dot{v} + h_u - J_u^\top f = 0 \tag{13a}$$

$$M_a \dot{v} + h_a - J_a^\top f = \tau \tag{13b}$$

Eq. (13a) is equivalent to the centroidal dynamics [15] and is sufficient to ensure dynamic consistency in the controllers based on Task-Space Inverse Dynamics (TSID) [4]. Finally, the relationship between the accelerations of the contact points and the robot configuration is given by:

$$\ddot{p} = J\dot{v} + \dot{J}v \tag{14}$$

III. FLEXIBLE TSID (TSID-FLEX-K)

This section presents our first original control formulation, which consists in a standard feedback linearization. In the case of visco-elastic contacts we cannot directly control f, but only its first or second derivative. As already mentioned, since we are mainly interested in underdamped contacts, we assume we can only control $\ddot{f}$. Thus, we differenciate (11) twice and use (4) to express $x^{(4)}$ as a function of $\ddot{p}$:

$$\begin{aligned} x^{(4)} &= A\ddot{f} + 2\dot{A}\dot{f} + \ddot{A}f = \\ &= \underbrace{(A_f - AK)}_{A_K}\ddot{p} + \underbrace{2\dot{A}\dot{f} - \ddot{A}_c f}_{a_K}, \end{aligned} \tag{15}$$

where:

$$\ddot{A}_c \triangleq \begin{bmatrix} 0_3 & \cdots & 0_3 \\ [\ddot{c}\times] & \cdots & [\ddot{c}\times] \end{bmatrix} \quad A_f \triangleq \begin{bmatrix} 0_3 & \cdots & 0_3 \\ [f_1\times] & \cdots & [f_k\times] \end{bmatrix} \tag{16}$$

A. Feedback Linearization

We can find the accelerations $\dot{v}$ that track at best the desired $x_d^{(4)}$ by solving the following least-squares problem [4]:

$$\begin{aligned} \underset{\dot{v}}{\text{minimize}} \quad & \|A_K J\dot{v} + A_K \dot{J}v + a_K - x_d^{(4)}\|^2 + \\ & w_{post}\|\dot{v}^{post} - \dot{v}\|^2 \\ \text{subject to} \quad & M_u\dot{v} + h_u = J_u^\top \hat{f} \\ & |M_a\dot{v} + h_a - J_a^\top \hat{f}| \leq \tau^{max} \end{aligned} \tag{17}$$

where $w_{post} \in \mathbb{R}$ is the weight of the postural task (typically much smaller than 1), $\hat{f} \in \mathbb{R}^{3k}$ are the measured/estimated contact forces, the first constraint represents the centroidal dynamics, and the second constraint represents the joint torque limits. The reference postural task accelerations are:

$$\dot{v}^{post} = K_p^{post} e_q(q^*, q) - K_d^{post} v, \tag{18}$$

where $K_p^{post}, K_d^{post} \in \mathbb{R}^{(n+6) \times (n+6)}$ are positive-definite diagonal gain matrices, $q^* \in SE(3) \times \mathbb{R}^n$ is a given reference posture, and $e_q(q_1, q_2)$ is an error function mapping two configurations $q_1, q_2 \in SE(3) \times \mathbb{R}^n$ to the log of their relative displacement. Once we have the optimal accelerations $\dot{v}_d$, we can compute the desired joint torques using (13b) with $\dot{v} = \dot{v}_d$ and $f = \hat{f}$.

B. Accounting for force variations during the time step

Since we can only update the motor commands at discrete time steps, there is always an error due to state variations inbetween time steps. Normally, these errors are negligible because small state variations result in small variations of the quantities in (13). However, when the robot is in contact with a stiff environment, small displacements of the contact points lead to large variations of the contact forces. Therefore, we can improve performance by accounting for the variation of f during the time step, assuming the following approximated time evolution:

$$f(t) = f + t\dot{f} \qquad t \in [0, \delta t], \tag{19}$$

where δt is the controller time step. Under this assumption the accelerations $\dot{v}$ vary during the time step. To get the desired average value of $\dot{v}$ during the time step the controller must compensate for the average value of f, which is:

$$f^{avg} = \hat{f} + \frac{\delta t}{2}\hat{\dot{f}} \tag{20}$$

In (17) we can thus replace $\hat{f}$ with $\hat{f} + \frac{\delta t}{2}\hat{\dot{f}}$.

C. Linear Feedback Regulator

The least-squares problem (17) allows us to directly impose $x^{(4)}$—if it is compatible with the problem constraints. Thus, the resulting dynamics is a 4-th order integrator. We define x as the centroidal state $x = (mc, l^\Sigma)$, where $l^\Sigma \in SO(3)$ should be the integral of the angular momentum. However, since this is not a measurable quantity [16], we approximate it with the orientation of the base link (which is typically the heaviest link), scaled by the 3D robot inertia. We then regulate x through a linear feedback control law:

$$\begin{aligned} x_d^{(4)} =& K_p^m e_x(x^*, x) + K_d^m(\dot{x}^* - \dot{x}) + \\ & K_a^m(\ddot{x}^* - \ddot{x}) + K_j^m(\dddot{x}^* - \dddot{x}) + x^{(4)*}, \end{aligned} \tag{21}$$

where $x^*(t)$ is a reference centroidal trajectory, and $e_x(x_1, x_2)$ is an error function mapping two centroidal states $x_1, x_2 \in SE(3)$ to the log of their relative displacement. The diagonal positive-definite feedback gain matrices $K_p^m, K_d^m, K_a^m, K_j^m \in \mathbb{R}^{6 \times 6}$ need to be chosen so that the closed-loop system be stable.

D. Friction Force Constraints

The inverse-dynamics least-squares problem typically contains a linear approximation of the force friction cone constraints. This is no longer possible in the case of visco-elastic contacts, because the contact forces are not a problem variable. However, we can still try to satisfy the friction cone constraints by bounding the contact force accelerations, which is an affine function of $\dot{v}$. This problem is similar to trying not to hit the joint position bounds by constraining the joint accelerations [17]. The friction cone constrains can be approximated by a set of linear constraints [4] of the form:

$$b^\top f_i \leq 0 \tag{22}$$

Using the approach of [17], given a bound on the force accelerations $\ddot{f}_{max} \in \mathbb{R}^3$ (i.e. $|\ddot{f}_i| \leq \ddot{f}_{max}$), we can compute the maximum $\dot{f}_i$ in direction b such that it is possible to satisfy (22) in the future:

$$b^\top \dot{f}_i \leq \sqrt{-2|b^\top \ddot{f}_{max}|(b^\top f_i)} \qquad (23)$$

Even though $\ddot{f}_{max}$ depends on q, the method that we use [17] assumes constant acceleration bounds. Therefore, $\ddot{f}_{max}$ should be seen here as a user parameter that defines how conservative the algorithm should be. Putting together all the friction cone constraints as $Bf \leq 0$ we can bound the force accelerations to ensure that (23) be satisfied at the next time step:

$$B\ddot{f} \leq b_f^{max}, \qquad (24)$$

where b_f^{max} is a function of f and $\dot{f}$ [17]. Finally, this constraint can be expressed as a function of $\dot{v}$:

$$-BK(J\dot{v} + \dot{J}v) \leq b_f^{max} \qquad (25)$$

E. Summary

The controller is finally obtained by adding (25) as a constraint to (17), with $x_d^{(4)}$ computed by (21).

IV. INVERSE DYNAMICS WITH RIGID CONTACTS (TSID-RIGID)

This section summarizes the classic approach for balancing a legged robot in rigid contact with the environment [4].

The desired momentum rate of change is typically computed with a simple PD control law:

$$\ddot{x}_d = \begin{bmatrix} m\ddot{c}_d \\ \dot{l}_d \end{bmatrix} = \begin{bmatrix} m\ddot{c}^* + K_d^{com}\dot{e}_c + K_p^{com}e_c \\ \dot{l}^* + K_d^{am}\dot{e}_l + K_p^{am}e_l \end{bmatrix}, \qquad (26)$$

where e_c and e_l are the tracking error of the linear and angular part of the centroidal state, respectively. Often, the proportional part of the angular momentum feedback is neglected, but we use it here to ensure stability [6]. The contact forces and the robot accelerations are computed by solving this least-squares problem:

$$
\begin{aligned}
\underset{\dot{v},f}{\text{minimize}} \quad & ||Af - \ddot{x}_d + b||^2 + w_f||f - f^*||^2 + \\
& w_{post}||\dot{v}^{post} - \dot{v}||^2 \\
\text{subject to} \quad & M_u\dot{v} + h_u = J_u^\top f \\
& J\dot{v} + \dot{J}v = 0 \\
& |M_a\dot{v} + h_a - J_a^\top f| \leq \tau^{max} \\
& Bf \leq 0,
\end{aligned}
\qquad (27)
$$

where $w_f \in \mathbb{R}$ is the weight and $f^* \in \mathbb{R}^{3k}$ is the reference of the force regularization task. Once the optimal contact forces f_d and robot accelerations $\dot{v}_d$ are found, we compute the desired joint torques using (13b). Note that, contrary to the other controllers, this approach does not require (nor exploit) any force measurement.

V. ADMITTANCE CONTROL (ADM-CTRL)

A classic way to control the contact wrenches in case of flexible contacts is to rely on admittance control. Several versions of admittance control exist and have been shown to perform well on real humanoid robots [18], [7], [8], [19]. We decided to use the version with the minimum number of gains to simplify the gain tuning procedure.

First, we compute the desired contact forces f_d as:

$$
\begin{aligned}
\underset{f}{\text{minimize}} \quad & ||Af - \ddot{x}_d + b||^2 \\
\text{subject to} \quad & Bf \leq 0,
\end{aligned}
\qquad (28)
$$

where $\ddot{x}_d$ is defined as in (26). We then compute the reference velocity of the contact points according to the force tracking error:

$$\dot{p}_d = -K_f(f_d - f) \qquad (29)$$

This reference velocity is directly used in a velocity-based inverse kinematics (IK) algorithm to compute reference joint velocities. The IK is computed on each limb independently:

$$\dot{q}_{jd} = (JS^\top)^\dagger \dot{p}_d \qquad (30)$$

These joint velocities are then integrated and given to the high-gain position controller, which computes the joint torque commands:

$$\tau_d = K_p^j(q_{jd} - q_j) - K_d^j\dot{q}_j \qquad (31)$$

VI. INVERSE DYNAMICS ADMITTANCE CONTROL (TSID-ADM)

To improve the performance of admittance control we suggest to integrate it with an inverse dynamics control law. Once we have computed $\dot{p}_d$ with (29), we compute the desired contact point accelerations as:

$$\ddot{p}^* = K_d^{adm}(\dot{p}_d - \dot{p}) \qquad (32)$$

Finally, we rely on an inverse-dynamics control law to track these contact point accelerations:

$$
\begin{aligned}
\underset{\dot{v}}{\text{minimize}} \quad & ||J\dot{v} + \dot{J}v - \ddot{p}^*||^2 + w_{post}||\dot{v}^{post} - \dot{v}||^2 \\
\text{subject to} \quad & M_u\dot{v} + h_u = J_u^\top \hat{f} \\
& |M_a\dot{v} + h_a - J_a^\top \hat{f}| \leq \tau^{max}
\end{aligned}
\qquad (33)
$$

VII. GAIN TUNING

The performance of each controller strongly depends on how well its gains are tuned. However, this is seldom considered in comparisons. Therefore, the ability of the user in tuning a specific controller (e.g., because of experience) may bias the results. To avoid this, this section presents a unified approach for tuning the controllers presented above. The key idea is to write down the closed-loop dynamics of the centroidal state as:

$$
\begin{aligned}
u(t) &= -\bar{K}(\theta)y(t) \\
\dot{y}(t) &= \bar{A}y(t) + \bar{B}u(t) + r(y(t)) \approx H(\theta)y(t)
\end{aligned}
\qquad (34)
$$

where y is a function of the robot state (q, v) that contains (at least) the centroidal state x and its first derivative $\dot{x}$, $H \triangleq \bar{A} - \bar{B}\bar{K}$ is the closed-loop transfer matrix, which is a

function of the gain parameters θ, and $r(y)$ is the residual nonlinear part of the dynamics. Our goal will be to derive (34) for each controller such that $r(y)$ is as small as possible (ideally null), so that we can neglect it and tune the gains for the resulting linear system. Once we have (34) we can look for a value of θ that solves the following optimal control problem:

$$
\begin{aligned}
\underset{\theta, y(t), u(t)}{\text{minimize}} \quad & \int_0^T [y(t)^\top Q y(t) + u(t)^\top R u(t)] \mathrm{dt} \\
\text{subject to} \quad & \dot{y}(t) = \bar{A} y(t) + \bar{B} u(t) \qquad \forall t \in [0, T] \quad (35) \\
& u(t) = -\bar{K}(\theta) y(t) \qquad \forall t \in [0, T] \\
& y(0) = y_0,
\end{aligned}
$$

where Q, R, T and y_0 are provided by the user. In the following we will assume that:

- the robot dynamical model is perfect,
- w_f and w_{post} are sufficiently small not to significantly affect the momentum task,
- the inequality constraints (e.g., friction cones) are not active.

Thanks to the last two assumptions, we can approximate the desired contact forces computed by (27) and (28) as:

$$
f_d = A_0^\dagger (\ddot{x}_d - b), \quad (36)
$$

where A_0 is the value of A computed at a reference configuration q_0.

A. TSID-Flex-K

This controller performs an exact feedback linearization, therefore the closed-loop dynamics of x is a 4-th order integrator, as shown by (21). Consequently, we can find the gain parameters $\theta = (K_p^m, K_d^m, K_a^m, K_j^m)$ using LQR.

B. Admittance Control

We could not find a proper way of linearizing the closed-loop dynamics for this case, so we have simply tuned the controller by hand.

C. TSID-Admittance

Let us define the state of the system as $y = (x, \dot{x}, f, \dot{f})$. The matrices $\bar{A}, \bar{B}, \bar{K}$ are defined as:

$$
\bar{A} = \begin{bmatrix} 0 & I & 0 & 0 \\ 0 & 0 & A_0 & 0 \\ 0 & 0 & 0 & I \\ 0 & 0 & 0 & 0 \end{bmatrix} \qquad \bar{B} = \begin{bmatrix} 0 \\ 0 \\ 0 \\ I \end{bmatrix} \quad (37)
$$

$$
\bar{K} = \begin{bmatrix} K_1 A_0^\dagger K_p^m & K_1 A_0^\dagger K_d^m & K_1 & K_d^a \end{bmatrix}
$$

where: $K_1 \triangleq K K_d^a K_f$. The gain parameters are $\theta = (K_d^a, K_p^m, K_d^m, K_f)$. Since we cannot freely choose $\bar{K}$ we should rely on global optimization to find θ. However, if we focus on the CoM only (i.e., neglecting the angular momentum), we can derive a simpler expression of the closed-loop dynamics, which allows us to use LQR. First of all, we assume that:

- contact damping is negligible: $B \approx 0$;
- K_d^{adm} and KK_f are diagonal matrices;
- all entries of K_d^{adm}, and KK_f corresponding to the same direction (X, Y, Z) have the same value; for instance, the admittance gain K_d^{adm} in direction Z must be the same for all contact points.

We can then define each of these matrices in terms of the 3d diagonal matrices K_d^{a3}, and K_f^3:

$$
\begin{aligned}
K_d^{adm} &= \text{diag}([K_d^{a3}, \quad \ldots, \quad K_d^{a3}]) \\
KK_f &= \text{diag}([K_f^3, \quad \ldots, \quad K_f^3])
\end{aligned} \quad (38)
$$

We define the state as $y = (c, \dot{c}, \ddot{c}, \dddot{c})$, and we get the following closed-loop dynamics:

$$
\bar{A} = \begin{bmatrix} 0 & I & 0 & 0 \\ 0 & 0 & I & 0 \\ 0 & 0 & 0 & I \\ 0 & 0 & 0 & 0 \end{bmatrix} \qquad \bar{B} = \begin{bmatrix} 0 \\ 0 \\ 0 \\ I \end{bmatrix} \quad (39)
$$

$$
\bar{K} = \begin{bmatrix} K_f^3 K_d^{a3} K_p^m & K_f^3 K_d^{a3} K_d^m & K_f^3 K_d^{a3} & K_d^{a3} \end{bmatrix}
$$

This closed-loop dynamics is equivalent to the one obtained by TSID-Flex-K (21), thus, we can find the desired gains using LQR.

D. TSID-Rigid

Since TSID-Rigid is a control scheme for a second-order system we define the state as $y = (x, \dot{x})$, and we get the following closed-loop dynamics:

$$
\bar{A} = \begin{bmatrix} 0 & I \\ 0 & 0 \end{bmatrix} \qquad \bar{B} = \begin{bmatrix} 0 \\ I \end{bmatrix} \quad (40)
$$

$$
\bar{K} = \begin{bmatrix} K_p^m & K_d^m \end{bmatrix}
$$

E. Cost Function

Ideally we would like to tune the gains of all controllers based on the same cost function. However, we do not have the same state for all controllers, in particular:

- for *TSID-Flex-K*, $y = (x, \dot{x}, \ddot{x}, \dddot{x})$ and $u = x^{(4)}$,
- for *TSID-Adm*, $y = (c, \dot{c}, \ddot{c}, \dddot{c})$ and $u = c^{(4)}$,
- for *TSID-Rigid*, $y = (x, \dot{x})$ and $u = \ddot{x}$.

Therefore, we start from a cost function for *TSID-Adm* defined by (Q, R):

$$
Q = \begin{bmatrix} I_3 & 0 & 0 & 0 \\ 0 & 0 & 0 & 0 \\ 0 & 0 & 0 & 0 \\ 0 & 0 & 0 & 0 \end{bmatrix} \qquad R = w_u I_3, \quad (41)
$$

where $w_u \in \mathbb{R}$ is a user-defined hyper-parameter. Now we have to find the equivalent cost functions for the other controllers. To do so, we introduce a matrix P that projects the state-control pair (y, u) of a given controller to the state-control pair of *TSID-Adm*. Once P is defined we can use it in the cost function of (35):

$$
\begin{bmatrix} y^\top & u^\top \end{bmatrix} P^\top \begin{bmatrix} Q & 0 \\ 0 & R \end{bmatrix} P \begin{bmatrix} y \\ u \end{bmatrix} \quad (42)
$$

For *TSID-Flex-K* we have:

$$
P = m^{-1} \text{diag}([I_{3 \times 6} \quad I_{3 \times 6} \quad I_{3 \times 6} \quad I_{3 \times 6} \quad I_{3 \times 6}]) \quad (43)
$$

where $I_{3\times 6}$ is a matrix that selects the first 3 elements of a 6d vector. Unfortunately, for *TSID-Rigid* it is not possible to have the same cost function because its state does not contain high-order derivatives as the other controllers, so we will use a different cost function:

$$Q = \begin{bmatrix} I_3 & 0 \\ 0 & 0 \end{bmatrix} \qquad R = w_u I_3 \tag{44}$$

VIII. ESTIMATION

The control method TSID-Flex-K requires an estimation of the CoM position, its first three derivatives, the angular momentum, and its first two derivatives. To estimate these quantities we suggest to rely on an Extended Kalman Filter (EKF), which is an extension of the approach presented in [20]. We define the state of the system as:

$$s = (c, \dot{c}, l, f, \dot{f}) \tag{45}$$

The continuous time system dynamics is:

$$\dot{s} = \begin{bmatrix} 0 & I & 0 & 0 & 0 \\ 0 & 0 & 0 & m^{-1}I^k & 0 \\ 0 & 0 & 0 & [(p-c)\times] & 0 \\ 0 & 0 & 0 & 0 & I^k \\ 0 & 0 & 0 & 0 & 0 \end{bmatrix} \begin{bmatrix} c \\ \dot{c} \\ l \\ f \\ \dot{f} \end{bmatrix} + \begin{bmatrix} 0 \\ w_{\ddot{c}} - g \\ 0 \\ 0 \\ u + w_u \end{bmatrix}, \tag{46}$$

where $w_{\ddot{c}}$ and w_u are the process noise on the CoM acceleration and the force accelerations, respectively, and:

$$I^k = \begin{bmatrix} I_3 & \dots & I_3 \end{bmatrix}$$
$$[(p-c)\times] = \begin{bmatrix} [(p_0 - c)\times] & \dots & [(p_{k-1} - c)\times] \end{bmatrix} \tag{47}$$

The system dynamics is linear, except for the angular momentum. The choice of modeling a noise on the CoM acceleration is motivated by the fact that the robot might get pushed, so we need to account for disturbances acting directly at the CoM acceleration level. The measurement model is:

$$s_{meas} = \begin{bmatrix} I & 0 & 0 & 0 & 0 \\ 0 & I & 0 & 0 & 0 \\ 0 & 0 & I & 0 & 0 \\ 0 & 0 & 0 & I & 0 \end{bmatrix} \begin{bmatrix} c \\ \dot{c} \\ l \\ f \\ \dot{f} \end{bmatrix} + \begin{bmatrix} w_c \\ w_{\dot{c}} \\ w_l \\ w_f \end{bmatrix} \tag{48}$$

Of course c, $\dot{c}$ and l are not directly measured, but they are computed from the encoder measurements and the floating-base state estimation. The estimation of the floating-base state typically relies on the IMU measurements and the kinematics of the limbs in contact [21]. Once we have an estimate of the state s, we can easily compute the quantities $\ddot{c}$, $\dddot{c}$, $\dot{l}$, and $\ddot{l}$, which are needed by our controller. Note that, assuming the contact damping B is sufficiently small, the contact point positions needed in (46) can be directly computed from the contact force measurements as:

$$p = p_0 - K^{-1}f \tag{49}$$

IX. RESULTS

This section presents simulation results to compare the different approaches discussed in the paper:

- TSID-Flex-K: a novel approach, see Section III.
- TSID-Rigid: a state-of-the-art approach, see Section IV.
- Adm-Ctrl: a state-of-the-art approach, see Section V.
- TSID-Adm: a novel approach, see Section VI.

TABLE I: Simulation parameters.

Symbol	Meaning	Value
δt_{sim}	Simulation time step	0.0001 s
δt_{ctrl}	Control time step	0.001 s
μ	Force friction coefficient	0.3
K	Contact stiffness	α 200000
ζ	Contact damping ratio	0.3
T	Simulation time	6 s

TABLE II: Controller Parameters. $\text{diag}(M_0)$ is the diagonal part of the mass matrix evaluated at $q(0)$.

Symbol	Controller	Meaning	Value
w_{post}	TSID-Flex-K	Postural task weight	0.3
w_{post}	TSID-Adm	Postural task weight	0.001
w_{post}	Adm-Ctrl	Postural task weight	0.001
w_{post}	TSID-Rigid	Postural task weight	0.01
w_f	TSID-Rigid	Force regularization weight	0.0001
K_p^m	Adm-Ctrl	Proportional momentum gain	30.7
K_d^m	Adm-Ctrl	Derivative momentum gain	10.3
K_p^j	Adm-Ctrl	Proportional joint position gain	$10^4 \text{diag}(M_0)$
K_d^j	Adm-Ctrl	Derivative joint position gain	$200 \text{diag}(M_0)$
K_f	Adm-Ctrl	Proportional force gain	0.008
K_p^{post}	All	Proportional posture gain	10
K_d^{post}	All	Derivative posture gain	6

TABLE III: EKF noise standard deviations.

Symbol	Meaning	Value
σ_c	CoM position measurement	1e-3
$\sigma_{\dot{c}}$	CoM velocity measurement	1e-2
σ_l	Angular momentum measurement	1e-1
σ_f	Force measurement	1
σ_u	Control	1e4
$\sigma_{\ddot{c}}$	CoM acceleration disturbance	10

TABLE IV: Sensor noise standard deviations (σ) and quantization errors (δ).

Symbol	Meaning	Value
σ_{fy}	Force sensor (Y axis)	1.3e-2
σ_{fz}	Force sensor (Z axis)	1.0
σ_ω	Gyroscope	6.4e-3
δ_{fy}	Force sensor (Y axis)	1.8e-2
δ_{fz}	Force sensor (Z axis)	7.3e-2
δ_ω	Gyroscope	1.0e-3
δ_q	Encoders	8.2e-5

A. Simulation Environment

We have carried out all our simulations using a simple 2D biped robot, which moves in the YZ plane. The Z direction is aligned with gravity, while the Y direction points sidewards. The robot is composed by two legs and a torso, and it has 4 actuated joints: two rotatory hip roll joints and two prismatic knee joints. The geometric and inertial parameters of the links have been taken from HRP-2's model. The simulation is based on a simple explicit Euler integration scheme, and all simulation parameters are listed in Table I. The robot has two point feet in contact with a visco-elastic ground. We have investigated different values for the contact stiffness $K = 2\alpha 10^5$, ranging from $\alpha = 0.01$ (i.e. soft) to $\alpha = 1$ (i.e. stiff), while keeping the same contact damping ratio.

B. Gain Tuning

For tuning the momentum gains we have used the gain tuning procedure for all controllers (except Adm-Ctrl) and for 7 values of w_u. These values are the same for TSID-Flex-K and TSID-Adm, and they are evenly spaced in logarithmic scale between 10^{-12} and 10^{-6}. For TSID-Rigid instead we have used values between $10^{-3.5}$ and $10^{-1.5}$. The other task gains and weights have been tuned by hand and are reported in Table II. We have set the weight of the postural task so that it would not significantly affect the primary momentum task.

C. Test Description

At first, we have tested the controllers in an ideal simulation, without any noise, modeling errors, and feeding the controller with the real robot state. Then we have repeated the tests in more realistic conditions by introducing:

- realistic encoder quantization errors and white Gaussian noise on force sensing and gyroscope (see Table IV);
- an EKF (explained in Section VIII) to estimate the robot state, with the covariances specified in Table III;
- limited torque bandwidth by filtering the desired joint torques with a first-order low-pass filter with a cut frequency of 30 Hz.[1]
- joint Coulomb friction of about 1% of the maximum joint force/torque (0.4 Nm for hip joints, and 4 N for knee joints).

In the following we will refer to the first kind of simulations as *noiseless*, and to the second kind as *noisy*.

D. Discussion

All the results are summarized by Fig. 1. Each plot shows the results of the four controllers for all the gain sets (1 for Adm-Ctrl and 7 for the other controllers), but for a specific contact stiffness (either soft, medium, or stiff) and a specific simulation type (either noiseless or noisy). The points missing in the plots are the ones that resulted in unstable simulations (i.e. *NaN* values). The plots highlight the trade-off between CoM tracking error (x axis), which measures how fast balance is recovered after an external perturbation, and average CoM snap (y axis), which quantifies both the CoM oscillations and the control effort.

1) Soft Contacts: In the noiseless simulations both TSID-Flex-K and TSID-Adm perform well, meaning that they achieve a good trade-off between state tracking and control effort. For lower feedback gains (i.e. higher position tracking errors) TSID-Flex-K and TSID-Adm achieve very similar performance, whereas for higher feedback gains they differ because of the ways in which they handle friction cones.

The unavoidable force tracking delay of admittance-control strategies is typically seen as an issue in the literature [3], [8], because it clashes with the assumption of second-order dynamics. However, if we accept a fourth-order dynamics for our system, we can see that this delay is not at all incompatible with good CoM tracking (as long as gains are properly tuned), as shown for instance in Fig. 2. The only downside of this delay is that it may lead TSID-Adm to violate friction cone constraints. Indeed, even though TSID-Adm constrains the desired forces inside friction cones, real forces may violate these constraints because of the tracking delay.

Adm-Ctrl performs reasonably well too, but less than TSID-Flex-K and TSID-Adm. On the contrary, TSID-Rigid is unstable for all the tested gain sets, except one, and even in this one case its performance is inferior to the other controllers (see Fig. 3).

In the noisy simulations things change remarkably. First, the performance of TSID-Flex-K and TSID-Adm gets worse, especially in terms of CoM snap, and in particular for lower feedback gains. Nonetheless, they remain the best controllers overall. Adm-Ctrl is only slightly affected by the introduction of noise, showing a remarkable robustness. Surprisingly, TSID-Rigid performs much better than in the noiseless case, showing a stable behavior with 3 gain sets, and getting a performance that is much closer to the Pareto front. To understand why, we have performed another test removing Coulomb friction (see Fig. 4). This test shows that Coulomb friction was the cause of the improved stability of TSID-Rigid, and of much of the performance deterioration of the other controllers.

2) Medium Contacts: In the noiseless case TSID-Flex-K and TSID-Adm perform well, similarly to the soft-contact case. Adm-Ctrl also performs well, resulting in just a slightly higher CoM snap than for soft contacts. The main difference w.r.t. the soft-contact case is that TSID-Rigid is stable for most gain sets (5 out of 7), even though it performs worse than the other controllers.

In the noisy simulations TSID-Flex-K becomes unstable for all feedback gains. TSID-Adm becomes unstable only for low feedback gains ($w_u \geq 10^{-9}$), but results in an increased CoM snap for higher gains. The performance of Adm-Ctrl and TSID-Rigid instead gets only slightly worse, showing a significant robustness. Out of the 7 Pareto-optimal points, 4 are associated to TSID-Rigid, and 3 to TSID-Adm.

Despite the performance of TSID-Rigid and TSID-Adm may seem comparable according to this plot, they are qualitatively different. Fig. 5 shows one example of contact forces generated by the two approaches. TSID-Rigid generates fast-changing forces because it immediately applies the joint torques needed to generate the desired contact forces, and given the relatively high contact stiffness, these joint torques quickly result in the desired force change. TSID-Adm instead generates forces with larger oscillations, but with lower frequencies, which may be preferable on real hardware.

3) Stiff Contacts: In the noiseless case we can already observe a significant performance deterioration for TSID-Flex-K and TSID-Adm, which are unstable for many more gain sets (2 and 4 out of 7, respectively). Nonetheless, they remain the best controllers in this scenario. This deterioration is due to the control frequency, which is insufficient for this contact stiffness, so the sampling starts affecting stability and performance. For high contact stiffnesses, performance
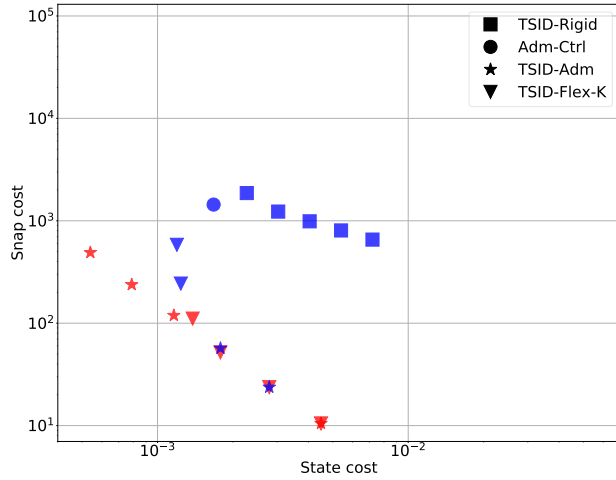
---

[1]The best torque-tracking bandwidths that have been reported for high-performance actuators are between 40 Hz and 60 Hz (e.g. 40 Hz for hydraulic actuators [2], 46 Hz for electric motors with harmonic drives [22], 60 Hz for series elastic actuators [23]).
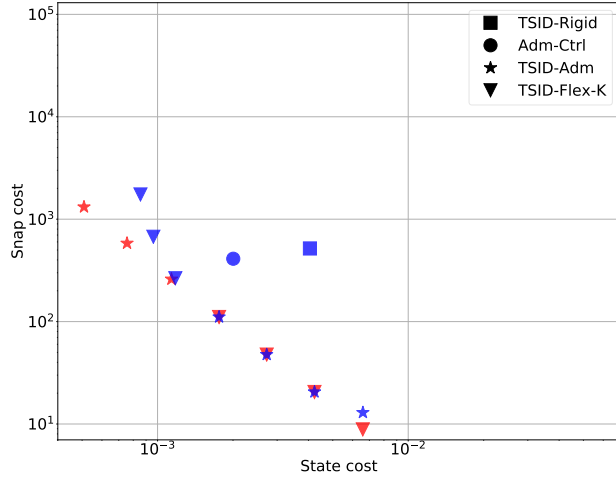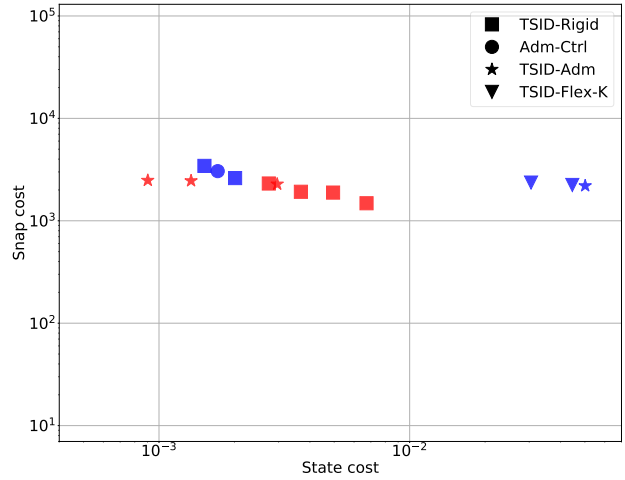
(a) Soft contacts ($\alpha = 0.01$), noiseless simulation.
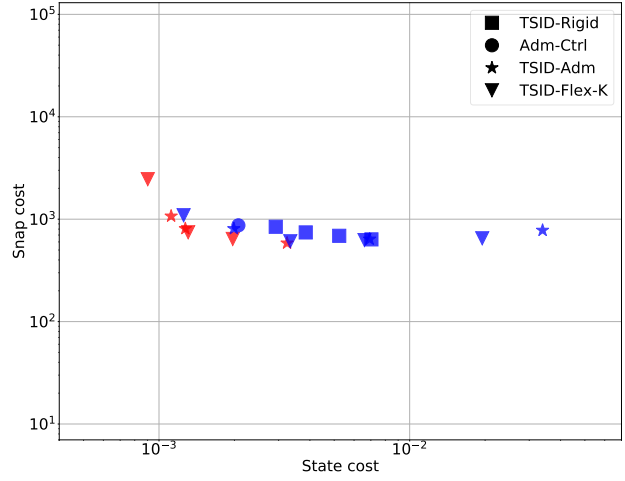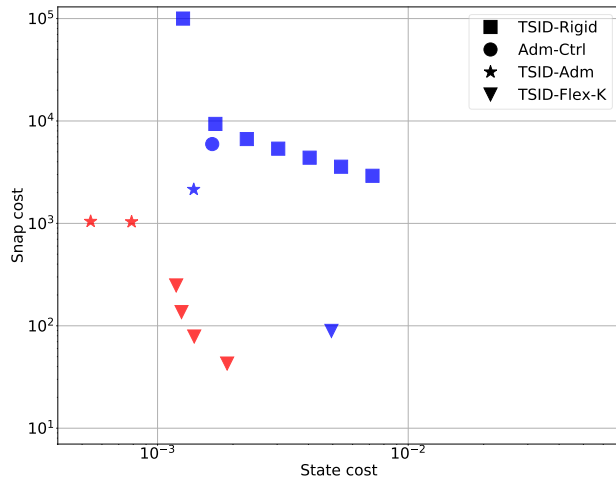
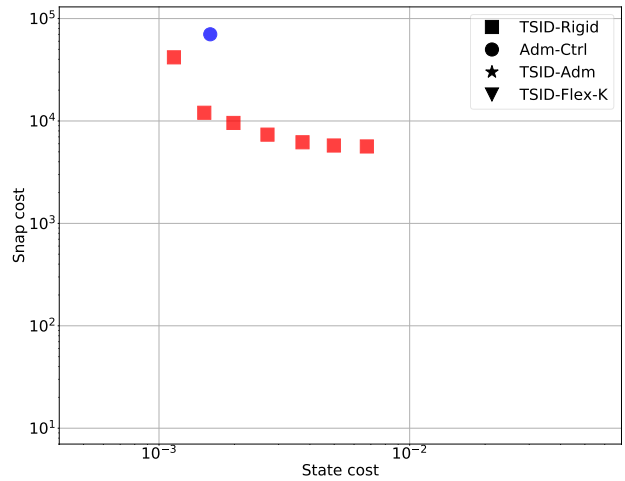(b) Soft contacts ($\alpha = 0.01$), noisy simulation.

(c) Medium contacts ($\alpha = 0.1$), noiseless simulation.

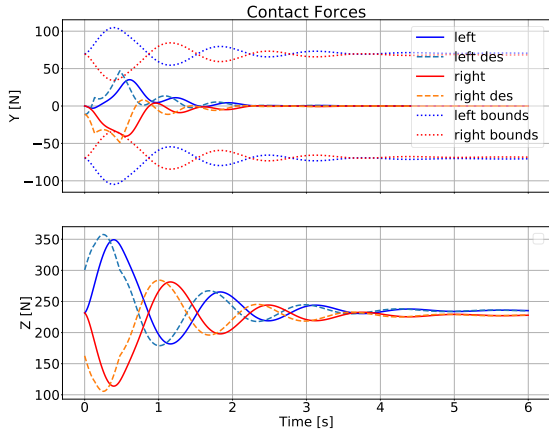(d) Medium contacts ($\alpha = 0.1$), noisy simulation.

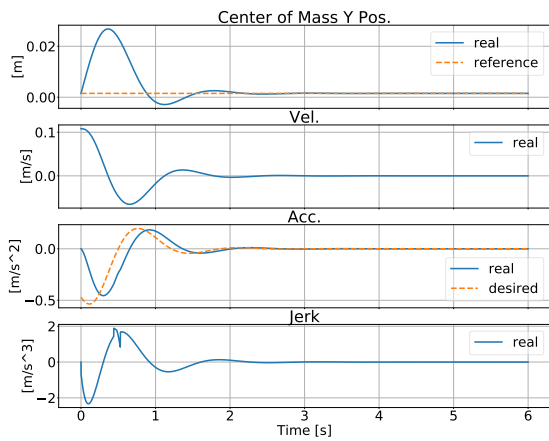(e) Stiff contacts ($\alpha = 1$), noiseless simulation.

(f) Stiff contacts ($\alpha = 1$), noisy simulation.

Fig. 1: Summary of all results. Pareto-optimal tests are depicted in red, while the others in blue.

(a) Contact force tracking.

(b) CoM trajectory.

Fig. 2: TSID-Adm, soft contacts ($\alpha = 0.01$), noiseless simulation and low feedback gains ($w_u = 10^{-6}$). CoM tracking is good despite the significant delay in force tracking.
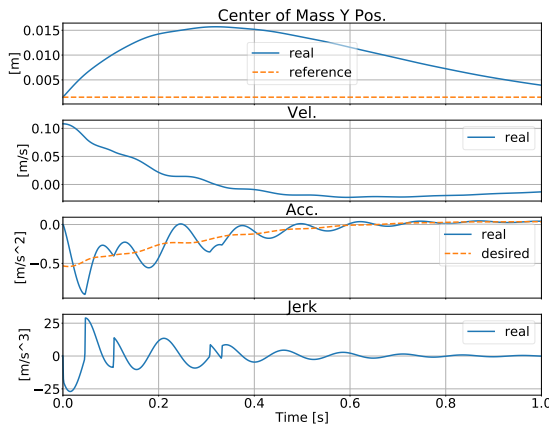
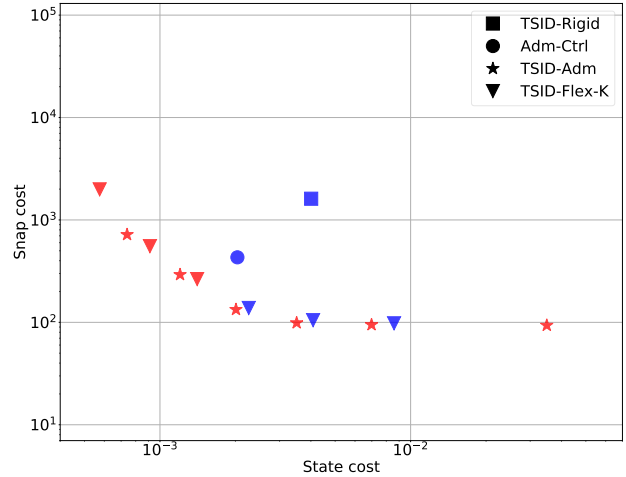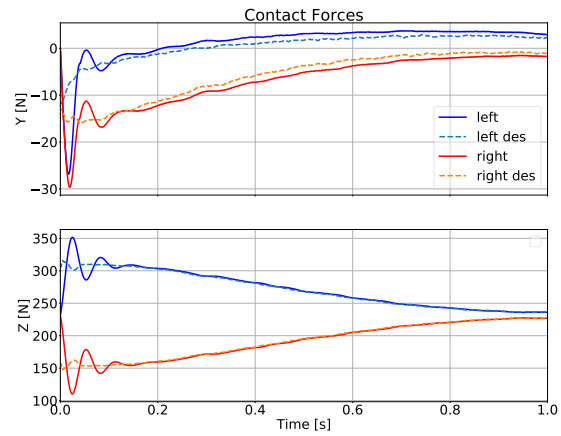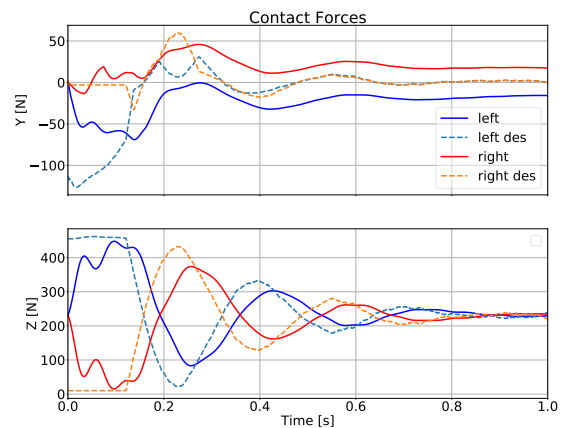Fig. 3: Performance of TSID-Rigid with soft contacts in noiseless simulation.

Fig. 4: Results for soft contacts ($\alpha = 0.01$) and noisy simulation, but without Coulomb friction. Coulomb friction has a detrimental effect to the performance of TSID-Flex-K and TSID-Adm, while it helps stabilizing TSID-Rigid.

(a) TSID-Rigid

(b) TSID-Adm

Fig. 5: Comparison between contact forces given by TSID-Rigid and TSID-Adm for medium contacts, noisy simulations.
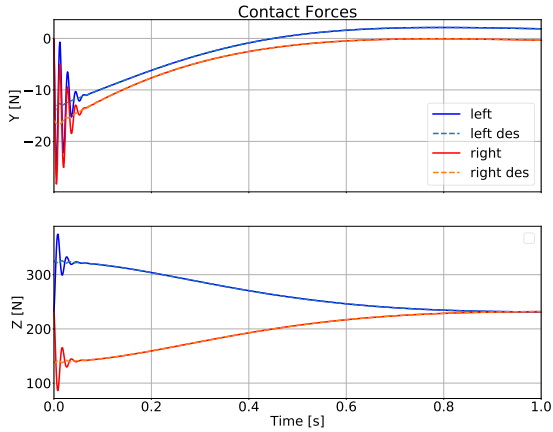
Fig. 6: Contact force generated by TSID-Rigid with stiff contacts, noiseless simulation.

could be improved by designing and tuning controllers in the discrete-time domain.

TSID-Rigid and Adm-Ctrl perform similarly to the medium-contact case: stable, but with high CoM snap. In particular TSID-Rigid results in high frequency oscillations of the contact forces (see Fig. 6), which may excite unmodelled dynamics (e.g., link flexibility) in real systems.

In the noisy case TSID-Flex-K and TSID-Adm became unstable for all gains. We believe that this is due to the delay in the compensation of the estimated contact forces, which triggers instability. This delay is caused by the limited joint torque bandwidth and the joint Coulomb friction.

TSID-Rigid and Adm-Ctrl remained stable, but their performance is far from satisfactory. Fig. 7 and 8 show the obtained CoM and force trajectories, which are extremely oscillatory (especially for Adm-Ctrl) and are thus unlikely to work on real hardware.

The interested reader is invited to watch the accompanying video for more details about the simulation results.

E. Summary

The presented results depict a broad picture of performance for 4 controllers, across 3 contact stiffnesses and 7 gain sets each (except for Adm-Ctrl, for which we have tested only one gain set). We highlight here our most interesting findings.

The novel controllers presented in this paper (TSID-Flex-K and TSID-Adm) perform really well for soft contacts, reasonably well for medium contacts, but they have showed instability for stiff contacts and noisy simulations.

TSID-Rigid has unsurprisingly shown the opposite trend, getting unstable for soft contacts (even though it was able to regain stability when introducing joint Coulomb friction), but then becoming more and more competitive as the contact stiffness increased. This is actually reasonable because the higher the contact stiffness, the more the system behaves as if contacts were rigid, which is a key assumption in TSID-Rigid.

One of the main advantages of the novel controllers is their ease of gain tuning, which allows for a unified tuning of force and position feedback gains (as acceleration/jerk gains can be seen as force gains). However, the novel controllers
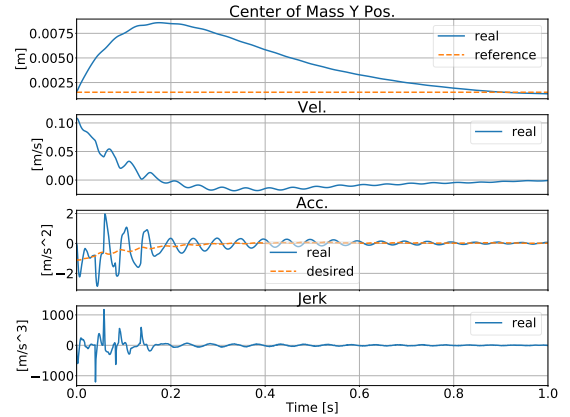
(a) Adm-Ctrl
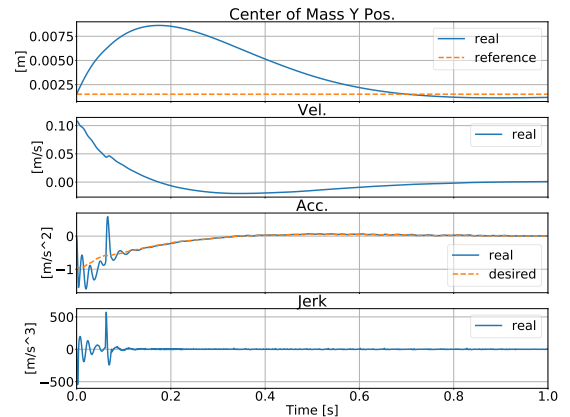
(b) TSID-Rigid

Fig. 7: Stiff contacts, noisy simulation.

have demonstrated a remarkable sensitivity to uncertainties. We believe that this is due to the attempt to compensate for the contact forces, which are rapidly changing (especially for stiff contacts), thus easily leading to destabilizing compensation errors. This makes these methods sensitive to low control frequencies and actuation delays, such as the ones introduced by limited joint-torques bandwidth and joint Coulomb friction.

Adm-Ctrl has been the only controller that was always stable, making it the most robust of them all. Despite its superior robustness, in no condition Adm-Ctrl has outperformed all of the other controllers. Moreover, its gain tuning remains a heuristic procedure, and its convergence properties are not yet clearly understood. All of this makes this controller hard to use in practice, highlighting the need for more work on this subject.

Overall, the case of stiff contacts was the hardest for the tested controllers: only TSID-Rigid and Adm-Ctrl remained stable, but they resulted in oscillatory trajectories, which are (at best) unpleasant on real hardware. These oscillations are due to the small contact damping, which combined with the high contact stiffness makes it really hard for the controller to damp the high frequency force oscillations.

Finally, these results show that controllers that are well supported by theoretical results and perform exquisitely in ideal conditions, can then fail miserably in realistic simula-
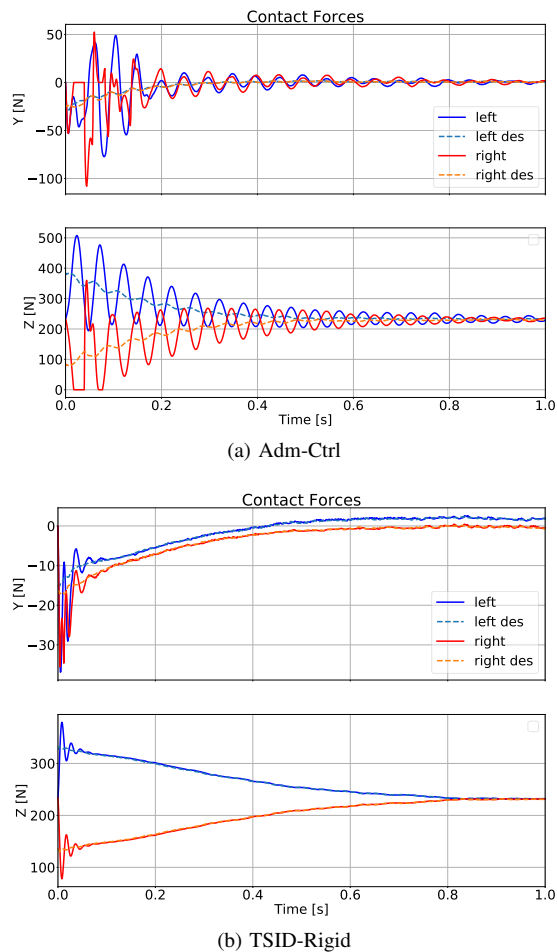
(a) Adm-Ctrl

(b) TSID-Rigid

Fig. 8: Stiff contacts, noisy simulation.

tions. Thus, working on robustness issues seems paramount for future work.

X. CONCLUSIONS

This paper presented a novel approach for balancing a legged robot on visco-elastic contacts. We have presented two novel control methods: TSID-Flex-K and TSID-Adm. To ensure a fair comparison between novel and state-of-the-art methods we have discussed a unified gain-tuning procedure (except for Adm-Ctrl, which we have tuned by hand).

Then, we have performed several tests in simulation using a simple 4-DoF robot. In these tests we have tried to span as many conditions as possible, covering different contact stiffnesses, different controller gains, and different simulation conditions (either noiseless or noisy). Our results highlight the challenges of this control problem and suggest that no controller is superior to all the others in all cases. Briefly, the two novel controllers performed well for soft/medium contacts, whereas TSID-Rigid was the best one for stiff contacts. Adm-Ctrl was the most robust, being the only one that never became unstable.

We believe that the subject of balance control on visco-elastic contacts will still require much investigation. We are especially interested in improving the robustness of the proposed

controllers, in the hope to find a better trade-off between performance and robustness. Another interesting direction could be to understand better the theoretical properties of Adm-Ctrl, which has clearly showed great robustness capabilities in our tests, but it remains unclear whether these capabilities can somehow be guaranteed in general.

REFERENCES

[1] P.-B. Wieber, R. Tedrake, and S. Kuindersma, "Modeling and Control of Legged Robots," in *Springer Handbook of Robotics*, 2nd ed., B. Siciliano and K. Oussama, Eds., 2015, ch. 48.

[2] T. Boaventura, C. Semini, J. Buchli, M. Frigerio, M. Focchi, and D. G. Caldwell, "Dynamic torque control of a hydraulic quadruped robot," *2012 IEEE International Conference on Robotics and Automation*, pp. 1889–1894, may 2012.

[3] J. Englsberger, C. Ott, and A. Albu-Schäffer, "Three-Dimensional Bipedal Walking Control Based on Divergent Component of Motion," *IEEE Transactions on Robotics*, vol. 31, no. 2, pp. 355–368, 2015.

[4] A. Herzog, N. Rotella, S. Mason, F. Grimminger, S. Schaal, and L. Righetti, "Momentum control with hierarchical inverse dynamics on a torque-controlled humanoid," *Autonomous Robots*, vol. 40, no. 3, pp. 473–491, 2016.

[5] H. O. Lim, S. A. Setiawan, and A. Takanishi, "Balance and impedance control for biped humanoid robot locomotion," in *IEEE International Conference on Intelligent Robots and Systems*, vol. 1, 2001, pp. 494–499.

[6] G. Nava, F. Romano, F. Nori, and D. Pucci, "Stability Analysis and Design of Momentum-based Controllers for Humanoid Robots," in *IEEE/RSJ International Conference on Intelligent Robots and Systems (IROS)*, 2016.

[7] T. Takenaka, T. Matsumoto, T. Yoshiike, T. Hasegawa, S. Shirokura, H. Kaneko, and A. Orita, "Real time motion generation and control for biped robot-4 th report: Integrated balance control," *IEEE/RSJ Int. Conf. on Intelligent Robots and Systems*, pp. 1601–1608, 2009.

[8] S. Kajita, M. Morisawa, K. Miura, S. Nakaoka, K. Harada, K. Kaneko, F. Kanehiro, and K. Yokoi, "Biped walking stabilization based on linear inverted pendulum tracking," in *Intelligent Robots and Systems (IROS)*, 2010, pp. 4489–4496.

[9] Z. Li, C. Zhou, Q. Zhu, and R. Xiong, "Humanoid Balancing Behavior Featured by Underactuated Foot Motion," *IEEE Transactions on Robotics*, vol. 33, no. 2, pp. 298–312, 2017.

[10] J. Reher, E. A. Cousineau, A. Hereid, C. M. Hubicki, and A. D. Ames, "Realizing dynamic and efficient bipedal locomotion on the humanoid robot DURUS," in *IEEE International Conference on Robotics and Automation*. IEEE, 2016, pp. 1794–1801.

[11] B. Henze, M. A. Roa, and C. Ott, "Passivity-based whole-body balancing for torque-conrolled humanoid robots in multi-contact scenarios," *The International Journal of Robotics Research*, vol. 35, no. 12, pp. 1522–1543, 2016.

[12] M. Azad and M. N. Mistry, "Balance control strategy for legged robots with compliant contacts," in *IEEE International Conference on Robotics and Automation*, 2015, pp. 4391–4396.

[13] S. Fahmi, C. Mastalli, M. Focchi, and C. Semini, "Passive Whole-Body Control for Quadruped Robots: Experimental Validation over Challenging Terrain," *IEEE Robotics and Automation Letters*, vol. 4, no. 3, pp. 2553–2560, 2019.

[14] S. Fahmi, M. Focchi, A. Radulescu, G. Fink, V. Barasuol, and C. Semini, "STANCE: Locomotion Adaptation over Soft Terrain," *IEEE Transaction on Robotics (under review)*, 2019.

[15] D. E. Orin, A. Goswami, and S.-H. Lee, "Centroidal dynamics of a humanoid robot," *Autonomous Robots*, vol. 35, no. 2-3, pp. 161–176, 2013.

[16] A. Saccon, S. Traversaro, F. Nori, and H. Nijmeijer, "On Centroidal Dynamics and Integrability of Average Angular Velocity," *IEEE Robotics and Automation Letters*, vol. 2, no. 2, pp. 943–950, 2017.

[17] A. Del Prete, "Joint Position and Velocity Bounds in Discrete-Time Acceleration / Torque Control of Robot Manipulators," *IEEE Robotics and Automation Letters*, vol. 3, no. 1, 2018.

[18] K. Hirai, M. Hirose, Y. Haikawa, and T. Takenaka, "The development of Honda humanoid robot," in *IEEE International Conference on Robotics and Automation*, 1998.

[19] S. Caron, A. Kheddar, and O. Tempier, "Stair Climbing Stabilization of the HRP-4 Humanoid Robot using Whole-body Admittance Control," in *arXiv preprint arXiv:1809.07073*, 2018.

[20] N. Rotella, A. Herzog, S. Schaal, and L. Righetti, "Humanoid momentum estimation using sensed contact wrenches," in *IEEE-RAS International Conference on Humanoid Robots*, 2015, pp. 556–563.

[21] T. Flayols, A. Del Prete, P. Wensing, A. Mifsud, M. Benallegue, and O. Stasse, "Experimental Evaluation of Simple Estimators for Humanoid Robots," in *IEEE International Conference on Humanoid Robots (Humanoids)*, 2017, pp. 889–895.

[22] H. Dallali, G. A. Medrano-Cerda, M. Focchi, T. Boaventura, M. Frigerio, C. Semini, J. Buchli, and D. G. Caldwell, "On the use of positive feedback for improved torque control," *Control Theory and Technology*, vol. 13, no. 3, pp. 266–285, 2015.

[23] N. Paine, S. Oh, and L. Sentis, "Design and Control Considerations for High-Performance Series Elastic Actuators," *IEEE/ASME Transactions on Mechatronics*, vol. 19, no. 3, pp. 1080–1091, 2014.